Article

A Bit-Interleaved Sigma-Delta-Over-Fiber Fronthaul Network for Frequency-Synchronous Distributed Antenna Systems

Chia-Yi Wu *,† , Haolin Li † , Joris Van Kerrebrouck , Caro Meysmans , Piet Demeester and Guy Torfs

IDLab, Department of Information Technology, Ghent University-imec, 9052 Ghent, Belgium;
haolin.li@ugent.be (H.L.); joris.vankerrebrouck@ugent.be (J.V.K.); caro.meysmans@ugent.be (C.M.);
piet.demeester@ugent.be (P.D.); guy.torfs@ugent.be (G.T.)
* Correspondence: chiayi.wu@ugent.be
† These authors contributed equally to this work.

Abstract: Cell-free massive multiple-input multiple-output (MIMO) has attracted wide attention as wireless spectral efficiency has become a 6G key performance indicator. The distributed scheme improves the spectral efficiency and user fairness, but the fronthaul network must evolve to enable it. This work demonstrates a fronthaul network for distributed antenna systems enabled by the bit-interleaved sigma-delta-over-fiber (BISDoF) concept: multiple sigma-delta modulated baseband signals are time-interleaved into one non-return-to-zero (NRZ) signal, which is converted to the optical domain by a commercial QSFP and transmitted over fiber. The BISDoF concept improves the optical bit-rate efficiency while keeping the remote unit complexity sufficiently low. The implementation successfully deals with an essential challenge—precise frequency synchronization of different remote units. Moreover, owing to the straightforward data paths, all transceivers inherently transmit or receive with fixed timing offsets which can be easily calibrated. The error vector magnitudes of both the downlink and uplink data paths are less than 2.8% (−31 dB) when transmitting 40.96 MHz-bandwidth OFDM signals (256-QAM) centered around 3.6 GHz. (Optical path: 100 m multi-mode fibers; wireless path: electrical back-to-back.) Without providing an extra reference clock, the two remote units were observed to have the same carrier frequency; the standard deviation of the relative jitter was 9.43 ps.

Keywords: 5G and beyond; 6G; cell-free massive MIMO; distributed antenna system (DAS); fronthaul network; next-generation radio access network (NG-RAN); radio-over-fiber (RoF); sigma-delta modulation (SDM)

1. Introduction

As communication systems evolve from one generation to another, the demands on system capacity, energy efficiency, and cost continuously become more challenging [1,2]. Massive multiple-input multiple-output (MIMO) is a key technology to increase wireless spectral efficiency and radiated energy efficiency for 5G [2–4]. 6G considers spectral efficiency as one of the key performance indicators (KPIs). It expects the peak spectral efficiency to double and the experienced spectral efficiency to increase tenfold [5]. Cell-free massive MIMO, also known as distributed massive MIMO, has attracted wide attention [2,5,6] because the distributed scheme can further improve the spectral efficiency and user fairness [7].

The fronthaul network evolution can be expected to enable cell-free massive MIMO. For mobile networks, high capacity, high scalability (in terms of the supported signal bandwidth and antenna number), low latency, and low deployment costs are always desirable. Most importantly, the network should provide precise synchronization between different remote units in both time and frequency [8].

For fronthaul networks, radio-over-fiber (RoF) technologies are among the most promising solutions owing to their high capacity and low latency [9]. Transmitting sigma-

delta modulated signals over fiber—sigma-delta-over-fiber (SDoF)—has been proposed as a feasible architecture combining the advantages of digitized RoF (DRoF) (higher linearity tolerances on both electrical and optical components) and analog RoF (ARoF) (simple remote unit architectures) [10]. Several SDoF-based fronthaul networks have been published [11–14].

This work demonstrates an SDoF-based fronthaul network in which multiple sigma-delta modulated baseband signals are time-interleaved and transmitted over fiber. Synchronization circuits are implemented to synchronize the frequency and lock the phase of the remote units of the distributed antenna system. Compared with our previous publications [12,13], more antennas can be served by one fiber while the complexity of remote units remains relatively low in contrast to those of DRoF-based networks.

A preliminary setup has been demonstrated online for the 46th European Conference on Optical Communication (ECOC 2020) [15]. This paper adds detailed design information and discusses the design trade-offs. It also includes measurement results to evaluate the system performance in various aspects.

The remainder of this article is organized as follows: Section 2 explains the core concept of the proposed network—bit-interleaved sigma-delta-over-fiber (BISDoF). Section 3 introduces the network architecture. In Section 4, we provide the measurement results with discussions, which show the achievable signal quality and validate the synchronization performance. Section 5 concludes the paper.

2. Bit-Interleaved Sigma-Delta-Over-Fiber (BISDoF)

The transmitted signals in SDoF links are sigma-delta modulated, i.e., oversampled and quantized to bi-level signals [16]. The generated quantization noise is shaped so that it falls outside the band of interest. Figure 1a shows the spectrum and waveform of a digitized 40.96 MHz-bandwidth orthogonal frequency-division multiplexing (OFDM) signal; both the in-phase (I) and quadrature (Q) signals are 16-bit. The baseband signals are modulated by second-order low-pass sigma-delta modulators (SDMs). Figure 1b shows the spectrum and the bi-level waveform of the sigma-delta modulated OFDM signal. The contained analog signals can be easily reconstructed from the modulated signals by filtering out the quantization noise.
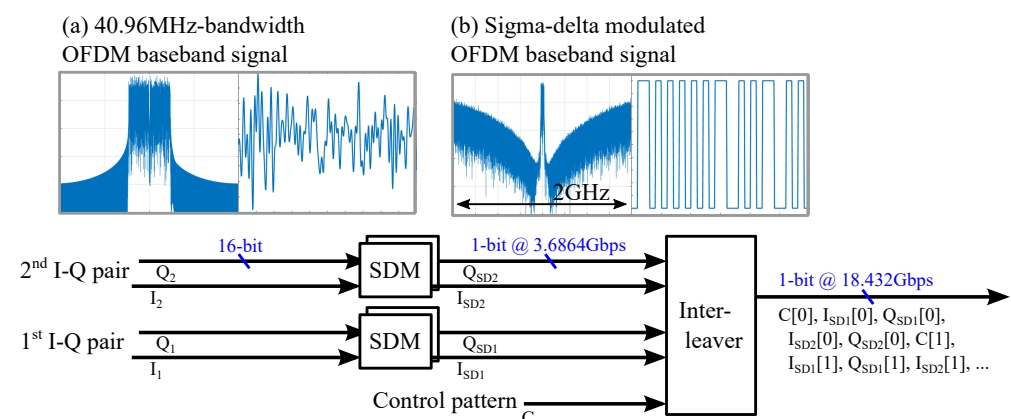

Figure 1. Bit-interleaved sigma-delta-over-fiber. (Gbps: gigabit per second.) (**a**) Spectrum and waveform of a 40.96 MHz-bandwidth OFDM baseband signal; (**b**) simulated spectrum and waveform of the sigma-delta modulated signal.

Instead of digitally up-converting [17] the signals to a radio frequency, as implemented in [12], or an intermediate frequency [13], four bi-level sigma-delta modulated baseband signals (corresponding to signals to/from two antennas) and one control sequence are interleaved into one BISDoF bitstream as illustrated in Figure 1. The control sequence contains either fixed patterns, which will later be used for de-interleaving, or commands. The bitstream is later converted into an optical non-return-to-zero (NRZ) signal and trans-

mitted over fiber. This architecture is used in both the downlink (DL) and uplink (UL) data paths of our proposed network.

The bi-level characteristic of the bitstreams allows for more relaxed linearity requirements on both optical and analog devices. Although the SDM sampling rate ($f_{\Sigma\Delta}$) is still high (3.6864 Gbps), the bit-rate efficiency, defined as

$$\text{bit-rate efficiency} = \frac{\text{signal bandwidth (MHz)}}{\text{optical bit-rate (Gbps)}}, \tag{1}$$

has improved 60% compared to our previous work [12] if 40.96 MHz-bandwidth signals are transmitted. In [12], the sigma-delta modulated I and Q signals are digitally up-converted [17] before being transmitted over fiber. To perform digital up-conversion, the bit rate must be four times the carrier frequency; therefore, the efficiency is 2.78 MHz/Gbps (40.96 MHz/(3.6864 Gbps × 4)). With BISDoF, the efficiency is 4.44 MHz/Gbps (40.96 MHz × 2/18.432 Gbps).

For the DL, the BISDoF bitstream from the central site is de-interleaved, 2×-up-sampled with the zero-order hold (ZOH) method, and digitally up-converted for the wireless transmission (Figure 2). The high $f_{\Sigma\Delta}$ is selected to match the carrier frequency (f_c) in order to maintain the simple DL data path at the remote unit.
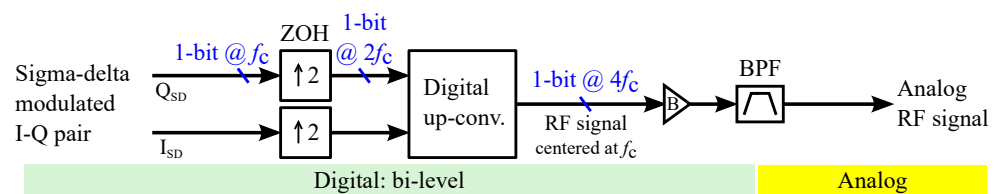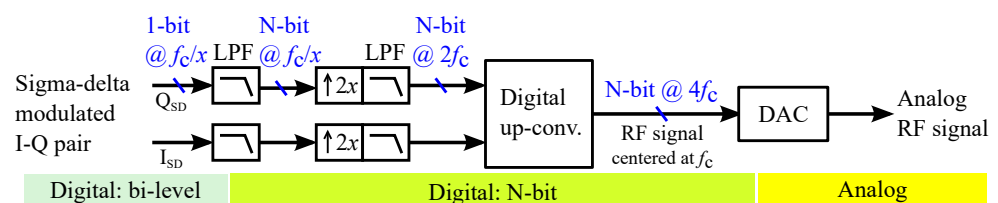

Figure 2. Converting the sigma-delta modulated I and Q signals into a radio-frequency (RF) signal for the downlink data path. (f_c: carrier frequency, 3.6864 GHz; ZOH: zero-order hold; ↑2: 2×-up-sampling; B: binary driver; BPF: band-pass filter.)

Choosing a lower $f_{\Sigma\Delta}$ can further increase the optical bit-rate efficiency. However, it would not be possible to simply apply the ZOH up-sampling because the quantization noise will be too close to the band of interest. Extra filters must be added to remove the quantization noise. Two possible architectures are depicted in Figure 3.
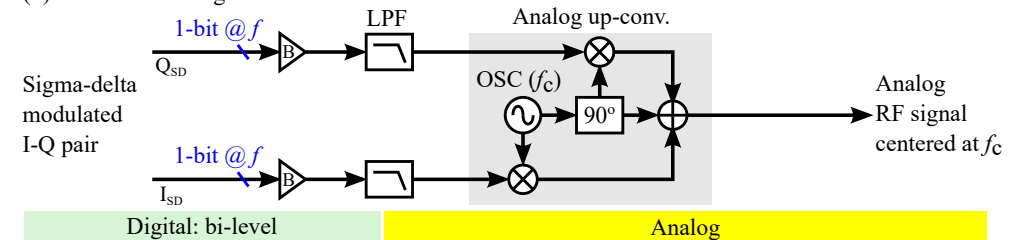

Figure 3. Two architectures with extra filters if a lower SDM sampling rate is chosen. (**a**) With extra digital filters; (**b**) with extra analog filters. (LPF: low-pass filter; DAC: digital-to-analog converter; OSC: oscillator.)

In Figure 3a, assume $f_{\Sigma\Delta}$ is lowered to f_c/x. After the first low-pass filter pair removes the quantization noise, the I and Q signals are no longer bi-level. These signals are $2x\times$-up-sampled and pass the anti-aliasing (low-pass) filters. Performing digital up-conversion requires the I and Q signals to be sampled at $2f_c$. Since the output signals are no longer bi-level, digital-to-analog converters (DACs) are required. If analog filters are added (Figure 3b), digital up-conversion is not possible and an analog up-converter must be included. In this option, $f_{\Sigma\Delta}$ can be chosen freely based on the signal quality requirement, thus simply denoted as f in the figure. Either way largely increases the complexity. It is a design trade-off between the optical bit-rate efficiency and the remote unit complexity.

For the UL, the de-interleaved signals are only down-sampled at the central site. It is indeed possible to lower $f_{\Sigma\Delta}$ and interleave more I-Q pairs in one fiber. For the ease of implementation, the proposed network has the same architecture for both directions.

3. System Architecture

Without loss of generality, Figure 4 illustrates the block diagram of a system with one central site and two remote units. The same figure has also been included in [15]. The terms "distributed unit (DU)" and "remote radio unit (RRU)" are aligned with the 5G next-generation radio access network (NG-RAN) terminology. It should be noted that the proposed architecture can be deployed for other networks connecting one central site and multiple remote sites, e.g., fiber-to-the-room (FttR) or customized radio access networks for hot spots.

The DU (Figure 5a) comprises a personal computer (PC) and a *Hitech Global* HTG-930 board, which connects to the PC via the peripheral component interconnect express (PCIe) interface and has a *Xilinx Virtex UltraScale+* FPGA (VU13P). (FPGA: field-programmable gate array.) The board is connected to a four-port QSFP FMC module. (QSFP: quad small form-factor pluggable; FMC: FPGA mezzanine card.) This PC is also used for performance monitoring. Each RRU (Figure 5b) consists of a *Xilinx Virtex Ultrascale* FPGA (VCU108) and an active antenna unit (AAU), which is in-house developed and has four wireless transceivers. The components used in the setup can be found in Appendix A. Although the block diagram seems complicated due to the provided details, the hardware is actually straightforward and can easily be incorporated in an application-specific integrated circuit (ASIC).

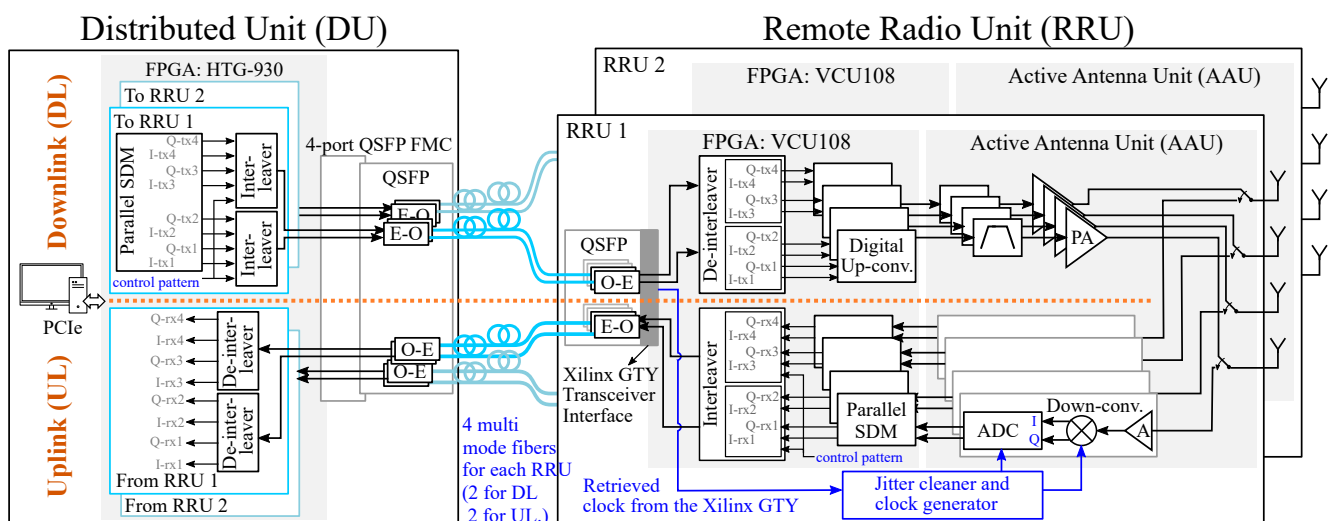**Figure 4.** Network architecture. (PCIe: peripheral component interconnect express; FPGA: field-programmable gate array; SDM: sigma-delta modulator; QSFP: quad small form-factor pluggable; FMC: FPGA mezzanine card; E-O/O-E: electrical-to-optical/optical-to-electrical converter; Up-/Down-conv.: up-/down-conversion; PA: power amplifier; A: low-noise amplifier; ADC: analog-to-digital converter.)
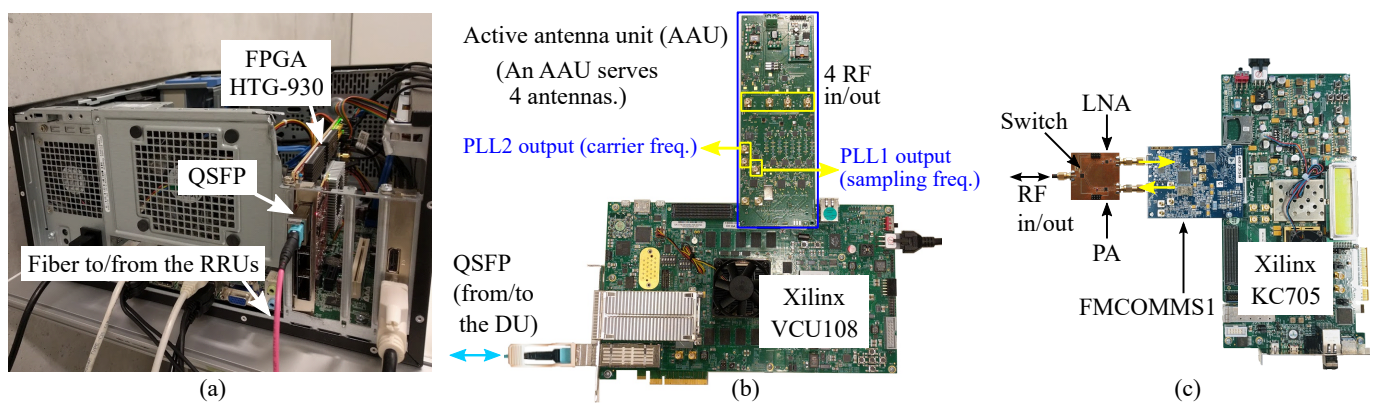
Figure 5. Photo of (**a**) the distributed unit (DU), (**b**) a remote radio unit (RRU), and (**c**) a user. The phase lock loop (PLL) outputs are used for debugging and performance monitoring.

The DU is connected to the RRUs with BISDoF links, in which baseband signals are sigma-delta modulated and time-interleaved before being transmitted over fiber, as explained in Section 2. Considering the targeted use cases and the implementation cost, this setup uses multi-mode fibers (MMFs) and commercial QSFP-100G-SR4 modules. Each QSFP has four 850 nm vertical-cavity surface-emitting lasers (VCSELs) and built-in clock-and-data recovery modules (CDRs) for transmitting and receiving. To serve all four transceivers on one RRU, two MMFs are used for the DL transmission and two others for the UL between the DU and each RRU.

If a longer transmission distance is required, single-mode fibers can be used instead. As NRZ signals are transmitted over fiber, the impact of fiber nonlinearities can be viewed as optical bit errors. Section 4.1 will further discuss the high bit error tolerance of sigma-delta modulated signals. Consequently, we expect similar performance.

A user (Figure 5c) has a *Xilinx Kintex 7* FPGA (KC705), an analog front end evaluation kit (*Analog Device* FMCOMMS1-EBZ), and a printed circuit board (PCB), which contains a low-noise amplifier (LNA) for reception, a power amplifier (PA) for transmission, and a switch.

3.1. Downlink Data Path

The downlink (DL) data goes first from the DU to an RRU via an optical link and then from an RRU antenna [18] to a user as shown in the upper half of Figure 4. The signals for transmission are provided to the DU FPGA by the PC via the PCIe interface; to collect the received signals for performance monitoring, the user is connected to the PC with Ethernet.

On the DU FPGA, sixteen parallel low-pass SDMs are implemented to serve two RRUs as four I-Q pairs are required by each RRU; the SDMs modulate the baseband signals at 3.6864 Gbps. Our previous work [19] has described the implementation of the real-time SDMs in detail. As illustrated in Figure 1, every four bi-level sigma-delta modulated signals, i.e., two pairs of sigma-delta modulated I and Q signals, are time-interleaved together with one bi-level control sequence into one NRZ signal, which is converted to the optical domain and transmitted over one fiber by a QSFP.

At each RRU, a QSFP converts the received 18.432 Gbps bitstreams from the optical domain to the electrical domain. On the FPGA, each bitstream is first de-interleaved back to two pairs of 3.6864 Gbps sigma-delta modulated I and Q signals; the signals are then up-sampled and digitally up-converted to the carrier frequency. Afterwards, band-pass filters on the AAU filter out the quantization noise. The radio-frequency (RF) signals are amplified and sent to antennas.

The DL data passes only simple and non-blocking modules; the signals are in fact streamed directly from the DU to all antennas. As a result, the transmit timing offsets between them, which may come from hardware mismatches or the locked phases of PLLs, are inherently fixed, although there is no absolute time shared between all transmitters.

Such offsets can either be calibrated or contained in the estimated channel information. The transmit timings can then be considered synchronous.

At the user, the received signals are amplified by the LNA, down-converted using a zero intermediate frequency (zero-IF) receiver, and sampled. The FPGA collects the sampled data whose quality is later checked by the PC.

3.2. Uplink Data Path

The uplink (UL) data goes from a user to RRUs wirelessly and then from RRUs to the DU via the optical links as depicted in the lower half of Figure 4. The transmitted data is loaded to the user via Ethernet. The FPGA streams the data to the FMCOMMS1-EBZ which converts the data to RF analog signals for transmission.

At an RRU, the AAU amplifies, down-converts, and samples the RF signals received by its antennas. The baseband signals, sampled at 92.16 MSps by the ADCs, are subsequently up-sampled and sigma-delta modulated at 3.6864 Gbps by the FPGA. Every two sigma-delta modulated I-Q pairs and one control sequence are time-interleaved and transmitted to the DU over one fiber. The DU QSFP converts the NRZ signals back to the electrical domain. The DU FPGA de-interleaves the electrical signals, filters out the quantization noise, and down-samples the signals to 81.92 MSps. The PC collects the data via the PCIe interface. Similar to the DL, the transparency of the data path guarantees that the UL data is received simultaneously by all antennas at RRUs and streamed directly to the DU.

A recently published work [14] proposes an SDoF-based system with all-digital pulse-width-modulation-based UL paths, whose RRU complexity is significantly lower. However, the UL signal quality degradation with respect to the DL is not negligible. The degradation may limit the possibility to exploit channel reciprocity [3].

3.3. Synchronization Circuit

To guarantee frequency synchronism between RRUs, a synchronization circuit is implemented on every AAU. For each RRU, the CDR module of the *Xilinx GTY* transceiver retrieves the clock information from the DL bitstreams and generates a 30.72 MHz clock. The retrieved 30.72 MHz clock goes to the AAU. However, the jitter of this clock is high due to the mediocre performance of the on-FPGA PLLs.

The synchronization circuit comprises two phase lock loops (PLLs) (Figure 6). The first PLL (PLL1) functions as a jitter cleaner and generates a low-jitter 92.16 MHz clock, which provides the sampling clock of analog-to-digital converters (ADCs) and the reference clock for the second PLL (PLL2). PLL2 generates the carrier clock for down-conversion. The measurement results in Section 4.2 demonstrate the RRU synchronism.
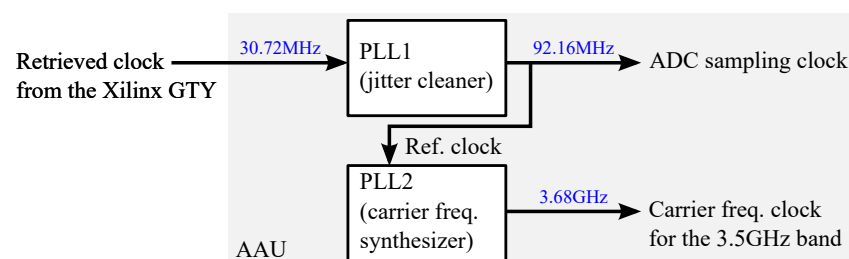
Figure 6. Block diagram of the synchronization circuit. (AAU: active antenna unit; ADC: analog-to-digital converter; PLL: phase lock loop.)

3.4. OFDM Signals

Python-generated OFDM baseband signals are used for both the DL and UL transmission for the ease of implementation and the possibility to experiment with physical layer signal processing.

The related parameters are listed in Table 1. The parameters are similar to those defined in the IEEE802.11ac specifications [20]. The signal bandwidth is selected to fit the

available ADC sampling rates. It should be noted that the proposed network architecture is standard agnostic. Digitized signals, which can be single-carrier or OFDM, with a bandwidth up to 40.96 MHz can be transmitted.

Table 1. OFDM Signal Parameters.

Data bandwidth	40.96 MHz
Subcarrier spacing	320 KHz
	128 subcarriers (index: −64 to 63)
Pilot subcarrier indices	±11, ±25, ±33
DC subcarrier indices	±1, 0
Null subcarrier indices	−64 to −59, 59 to 63
Number of data subcarriers	108
Cyclic prefix (CP) size	1/4 (0.78 us)
Modulation scheme	256-QAM (quadrature amplitude modulation)

4. Experimental Methodology and Measurement Results

Through extensive measurements, this section demonstrates two main advantages of the proposed architecture: (1) BISDoF links can deliver good quality data, which meets the 3GPP error vector magnitude (EVM) requirement for 256-QAM (3.5%) [21]; (2) the BISDoF-based network guarantees the frequency synchronism between RRUs without an extra reference clock signal provided.

4.1. Link Performance

The link performance was measured by transmitting 40.96 MHz-OFDM signals (256-QAM) centered at 3.6864 GHz. The root-mean-square EVM values provided in this paper are normalized to the average constellation power.

1. DL: from the DU to an RRU via an optical link with different fiber lengths, then from an RRU antenna to a user (electrical back-to-back);
2. UL: from a user to an RRU antenna (electrical back-to-back), then from the RRU to the DU via an optical link with different fiber lengths.

The combined length of the break-out fibers, and therefore the fiber length of the optical back-to-back cases, was about 8 m. The RF in/out ports of the RRU and the user were connected directly with a cable. Appropriate attenuation was applied to prevent the receiver chains from saturation. No reference clock was provided; the carrier frequency offset was estimated and canceled using the algorithm proposed in [22].

4.1.1. Downlink Performance

Table 2 lists the measured EVM values corresponding to different DL fiber lengths. Due to the high bit-error rate (BER) tolerance of sigma-delta modulated signals [23], there is little performance degradation when the optical transmission distance increases. While CPRI requires a BER less than 10^{-12} [24], a BER higher than 10^{-4} can be tolerated in SDoF applications; the corresponding signal quality is about −45 dB EVM [23]. The constellation diagram of the worst case—with a 100 m MMF added between the break-out fibers—can be found in Figure 7a.

Table 2. Downlink performance in EVM.

	DL (DU to RRU) Fiber Length		
	Back-to-Back	**30 m MMF**	**100 m MMF**
EVM	2.725% (−31.29 dB)	2.752% (−31.21 dB)	2.765% (−31.17 dB) Constellation: Figure 7a.

(a) **Downlink (DL) Performance**
DL fiber length: 100m

EVM: 2.765% (−31.17dB)

(b) **Uplink (UL) performance**
DL fiber length: back-to-back
UL fiber length: 100m

EVM: 2.684% (−31.42dB)

(c) **Uplink (UL) performance**
DL fiber length: 100m
UL fiber length: 100m
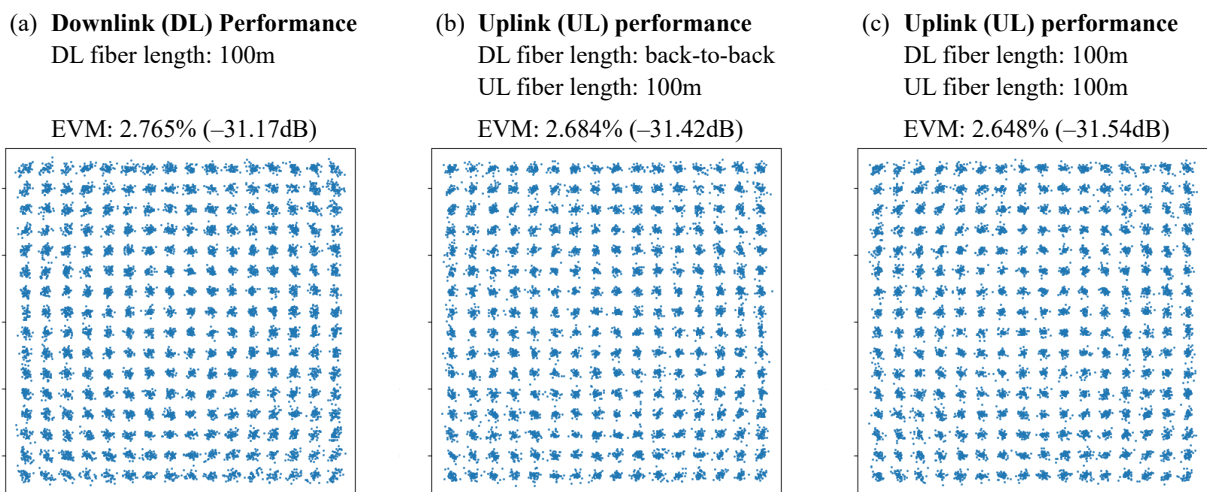
EVM: 2.648% (−31.54dB)

Figure 7. Constellation diagrams of the demodulated OFDM signals of the worst cases of the downlink (Table 2) and uplink performance measurements (Table 3).

4.1.2. Uplink Performance

Pseudorandom binary sequences (PRBSs) were transmitted over the DL fiber to keep the CDR locked. Therefore, the DL fiber length is expected to have an impact on the phase noise of the retrieved clock. Two scenarios with different DL fiber lengths were considered when measuring the UL performance: (1) back-to-back (2) with a 100 m MMF. Table 3 lists the measured EVM values corresponding to different UL fiber lengths under these two scenarios. Figure 7b and c show the corresponding constellation diagrams.

Table 3. Uplink performance in EVM.

| | UL (RRU to DU) Fiber Length | | |
	Back-to-Back	30 m MMF	100 m MMF
DL Back-to-Back	2.615% (−31.65 dB)	2.672% (−31.46 dB)	2.684% (−31.42 dB) Constellation: Figure 7b
DL 100 m MMF	2.621% (−31.63 dB)	2.641% (−31.56 dB)	2.648% (−31.54 dB) Constellation: Figure 7c

As in Table 2, there is little performance degradation when the UL optical transmission distance increases. The performance difference between the two scenarios is also negligible because the first PLL (PLL1) in Figure 6 properly cleans up the jitter.

4.2. RRU Synchronism

Three experiments were performed to demonstrate the RRU synchronism. The jitter measurement (Section 4.2.1) showed the carrier frequency stability over time and provided the asynchronous jitter information in the time domain. The spectrum measurement (Section 4.2.2) illustrated the asynchronous phase noise spectrum in the frequency domain. The last one calculated the phase difference between two RRUs using the estimated channel frequency responses.

4.2.1. Jitter Measurement

The DL bitstream contained PRBSs to keep the CDRs on both RRUs locked. The carrier frequency clocks of both RRUs were connected to the real-time oscilloscope (RTO) (*Lecroy LabMaster* 10-65Zi-a). RRU1's clock (labeled in yellow) was the trigger signal. Figure 8 shows the experiment setup and the results averaged over 20 s (the longest limited average duration of the RTO).
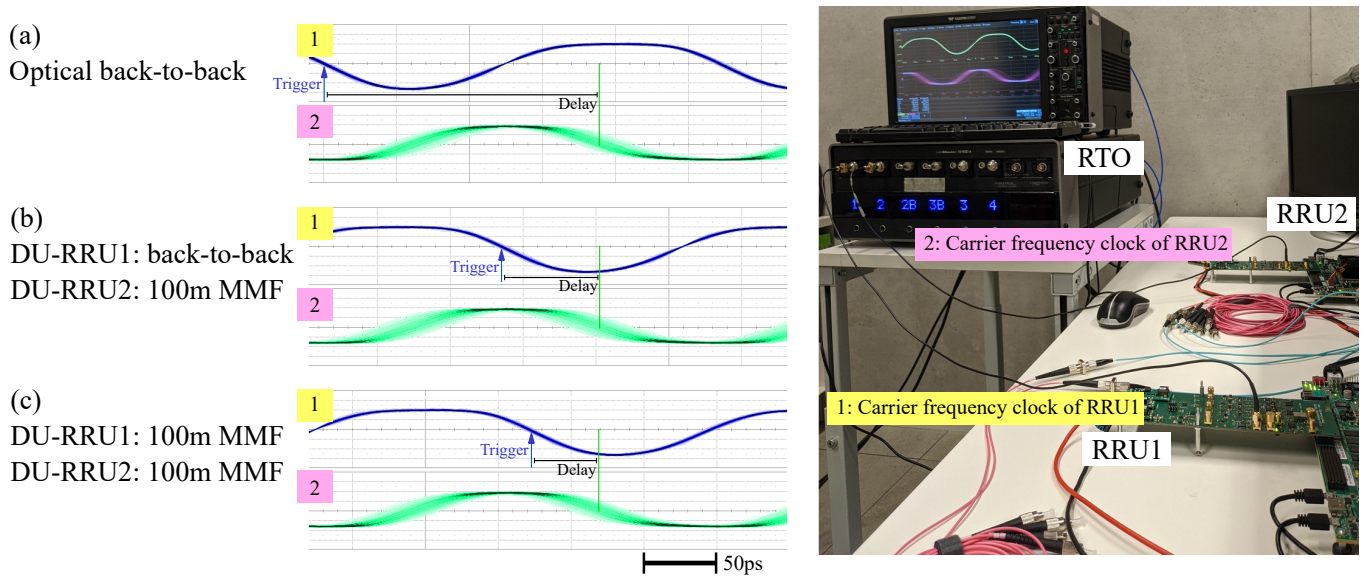
Figure 8. Jitter measurement setup and results. The results are shifted horizontally to align the edges of RRU2's clock (labeled in pink) for easy comparison. (RTO: real-time oscilloscope.)

The stable waveforms imply that the RRUs were frequency-synchronized owing to the synchronization circuits (Figure 6).

The RTO measured the delay between a falling edge of the trigger signal (RRU1's carrier frequency clock) and the first subsequent falling edge of the observed signal (RRU2's carrier frequency clock, labeled in pink) as marked in Figure 8. The mean values of the delay, indicating the average phase differences between two clock sources, were different for the three test scenarios because the PLLs had to re-lock each time we changed the fibers. Once the PLLs were locked, these mean values were stable and would be captured as the channel information. Hence, while the mean values remain stable, the transceiver coherency is guaranteed.

The standard deviation can be considered as an indicator of the asynchronous jitter. For the optical back-to-back case (Figure 8a), the standard deviation was 7.69 ps. After a 100 m MMF was added to only the RRU2 DL optical link (Figure 8b), the standard deviation increased to 9.11 ps. When the DL optical links of both RRUs had 100 m MMFs, the standard deviation increased slightly to 9.43 ps.

4.2.2. Spectrum Measurement

To measure the spectrum of the asynchronous phase noise, a 5 MHz sine wave modulated at the carrier frequency (3.6864 GHz), i.e., a 3.6914 GHz sine wave, was connected to one of the RF-in connectors of both RRUs with cables as illustrated in Figure 9.
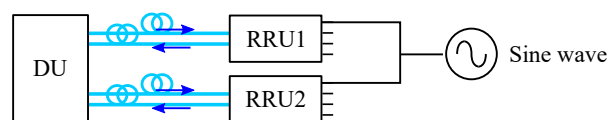

Figure 9. Measurement setup.

The DU provided PRBSs to keep the CDRs at the RRUs locked and received one sine wave from each RRU, sampled at 81.92 MSps; the sequences are about 25 ms long. A phase shift was applied to one sine wave and this phase-shifted sine wave was used to cancel the other sine wave. The spectrum of the cancellation result can be viewed as the asynchronous phase noise spectrum.

Figure 10 includes the results of two test scenarios, back-to-back and with a 100 m DL fiber. There is little noticeable difference between the two results. If the received sine

wave spectra of both scenarios are plotted together, the back-to-back case (Figure 10a) has slightly less phase noise.
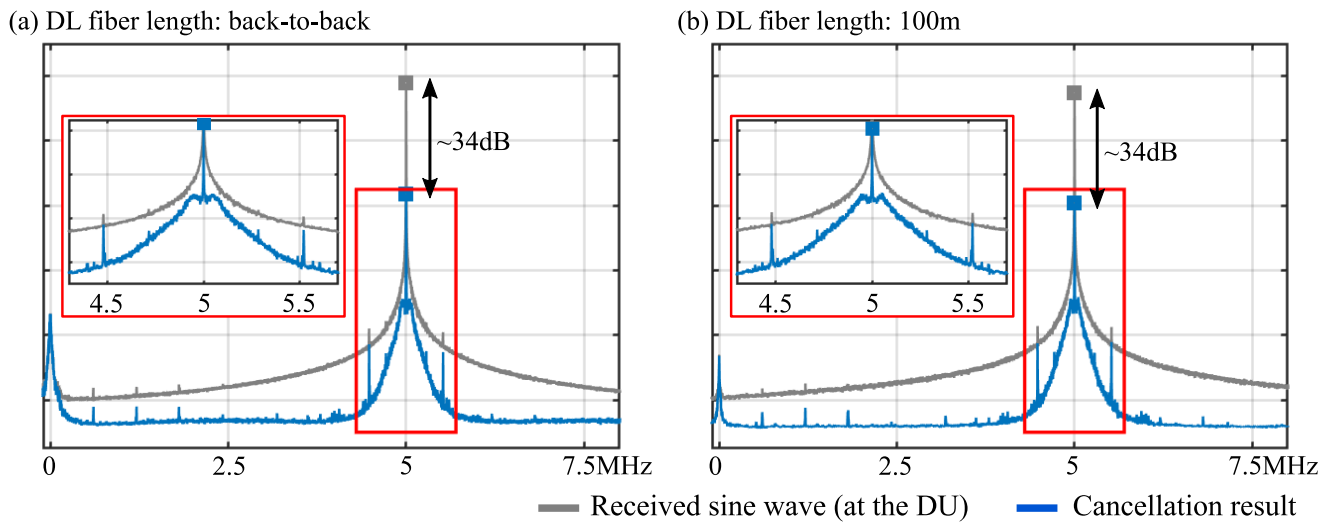
(a) DL fiber length: **back-to-back**　　　　　　　　　　(b) DL fiber length: 100m

Figure 10. Spectra of the received sine wave and the asynchronous phase noise. Measurement time duration: 25 ms.

About 34 dB suppression was reached for both scenarios. For each scenario, if we compare the two spectra, we can see that the phase noise contained in the two sine waves is mainly correlated. The correlated phase noise originated from the sine wave generator and the retrieved 30.72 MHz clocks, which were extracted from the DL bitstreams generated with one common reference clock at the DU. The spikes at 5 MHz $\pm$ 500 KHz were caused by the power supplies of the AAUs.

A similar figure has been published in [15]. The results are slightly different because the loop filters of the PLLs have been adjusted for better stability.

4.2.3. Phase Difference Measurement

Since distributed antenna systems are one of the targeted use cases for BISDoF-based networks, plotting the phase difference between two RRUs versus time gives an intuitive view of the achievable performance.

As illustrated in Figure 11, one RRU1 transceiver functioned as a transmitter, while another RRU1 transceiver and one RRU2 transceiver received the transmitted signal wirelessly. The two receivers were perfectly synchronized in sampling timing, carrier frequency, and sampling clock frequency. Instead of PRBS, an OFDM signal was sent to RRU1 via the DL fiber.
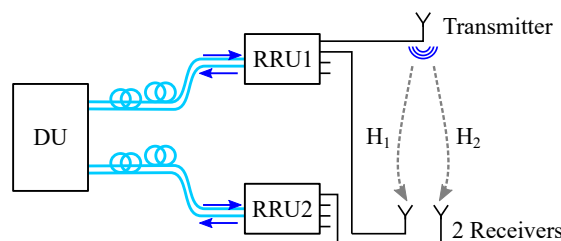

Figure 11. Measurement setup.

The overall channel frequency responses, $\mathbf{H}_1$ and $\mathbf{H}_2$, were estimated using the least square channel estimation in [25]. The estimation results, $\hat{\mathbf{H}}_1$ and $\hat{\mathbf{H}}_2$, both contain 128 complex values corresponding to 128 subcarriers.

During the measurement period, the wireless channels were assumed to remain static. The phase difference between the two RRUs, caused by the asynchronous jitter/phase noise, can be calculated by

$$\phi = \frac{1}{N_\mathbf{D}} \sum_{k \in \mathbf{D}} \text{angle}\left(\frac{\hat{H}_{1,k}}{\hat{H}_{2,k}}\right) \tag{2}$$

where k denotes the subcarrier index, $\mathbf{D}$ is the index set of all non-zero subcarriers and $N_\mathbf{D}$ is the number of indices in $\mathbf{D}$. $\hat{H}_{1,k}$ is the k-th element of $\hat{H}_1$.

Figure 12 plots ϕ versus time. The box plots of ϕ are included to better visualize the distribution. As in Section 4.2.1, the PLLs had to re-lock each time we changed the fibers, hence the change in the average phase difference. The average was observed to be stable once the PLLs were locked and would be contained in the overall channel frequency responses.

For the back-to-back case, the standard deviation of ϕ is 6.28°; 50% of the values fall within the range of the box: $-7.4°$ and 1.1° (a range of 8.5°). The data range excluding outliers is 31.5°. For the 100 m case, the standard deviation is 6.44°; 50% of the values are between 21.8° and 31.1° (a range of 9.3°). The data range excluding outliers is 31.2°.

The back-to-back case might seem to have a slightly better result. However, it is important to mention that the performance difference could come from both the DL signal quality and the retrieved clock quality. Overall, it can be concluded that the fiber length does not cause significant performance degradation.

Compared to co-located antenna systems in which little asynchronous phase noise is expected between transceivers, the fluctuation in phase difference can definitely degrade the digital beamforming accuracy. However, the rich spatial diversity brought by distributed schemes is expected to compensate for this drawback.
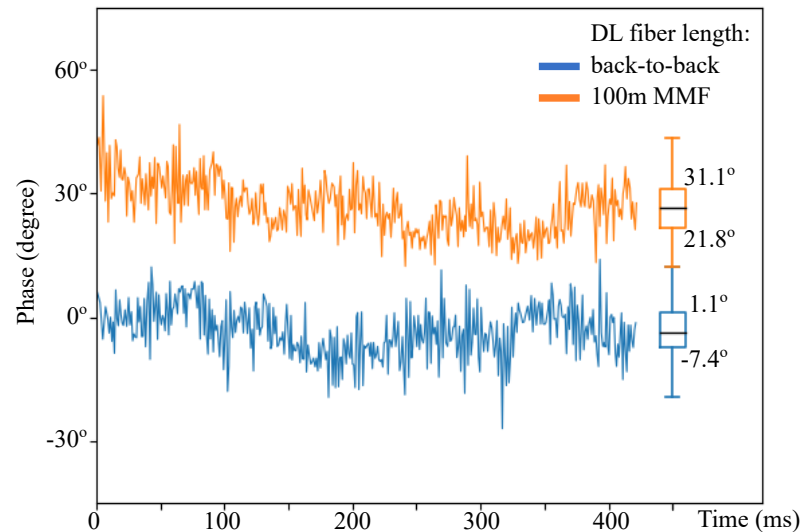

Figure 12. RRU phase difference versus time and its distribution.

4.3. Future Work

This work focuses on the BISDoF-based network, of which the performance has been comprehensively discussed. We are currently evaluating the performance of time division duplex (TDD) reciprocity calibration and digital beamforming with over-the-air measurements. The results are expected to be published in the near future.

5. Conclusions

This work proposes a competitive fronthaul solution for distributed antenna systems. Detailed design information and the reasons behind our design trade-offs are included. The system has good signal qualities for both the downlink and uplink data paths. Time-interleaving multiple sigma-delta modulated baseband signals into one bitstream allows

for the transmission of non-return-to-zero (NRZ) signals over fiber. It also keeps the remote unit complexity low while improving the optical bit-rate efficiency by 60% compared to our previous work.

The downlink and uplink performance satisfies the 3GPP error vector magnitude (EVM) requirement for 256-QAM (3.5%): the EVM of 40.96 MHz-bandwidth OFDM signals centered around 3.6 GHz is 2.765% (-31.17 dB) and 2.648% (-31.54 dB), respectively. (Optical path: 100 m multi-mode fibers; wireless path: electrical back-to-back.) Additionally, without an extra reference clock signal provided for synchronization, the network guarantees fixed transmit and sampling timing offsets between all transceivers and synchronizes the carrier and sampling frequencies between remote units. The synchronism is thoroughly validated with measurements in different domains. The real-time oscilloscope observation shows that the two remote units have the same carrier frequency and the standard deviation of the relative jitter is 9.43 ps during the 20-second measurement period.

In summary, as cell-free massive MIMO gains more attention, the proposed network architecture has a high potential for its good signal quality, guaranteed synchronism, and scalability.

Author Contributions: Conceptualization, H.L., P.D. and G.T.; hardware design (including implementation and verification), C.-Y.W., H.L., J.V.K. and C.M.; software design (offline signal processing), C.-Y.W.; system validation and experiment methodology, C.-Y.W., H.L. and J.V.K.; experiment result analysis, C.-Y.W.; resources, P.D. and G.T.; writing—original draft preparation, C.-Y.W.; writing—review and editing, H.L., J.V.K., C.M., P.D. and G.T.; supervision, G.T.; project administration, P.D. and G.T.; funding acquisition, P.D. and G.T. All authors have read and agreed to the published version of the manuscript.

Data Availability Statement: All results have been provided in the manuscript. The generated signals for performance measurements and part of the collected raw data are available on request.

Conflicts of Interest: The authors declare no conflict of interest. The funders had no role in the design of the study; in the collection, analyses, or interpretation of data; in the writing of the manuscript, or in the decision to publish the results.

Appendix A

Table A1 lists all commercial components used in the setup.

Table A1. Hardware Components.

QSFP	QSFP-100G-SR4 (850 nm)
Fiber	OM4 multi-mode
Remote radio unit (active antenna unit)	
switch	*Analog Devices* HMC8038
band-pass filter	*Mini-Circuits* BFCV–3641+
power amplifier	*Analog Devices* HMC327
low-noise amplifier	*Mini-Circuits* PMA3-83LNW+
down-converter	*Analog Devices* ADL5380
analog-to-digital converter	*Analog Devices* AD9633
crystal oscillator	*Crystek* CVHD–950–122.880
phase lock loop (PLL)	
PLL1 (Figure 6)	*Analog Devices* AD9524
PLL2 (Figure 6)	*Analog Devices* ADF4356

Table A1. *Cont.*

User	
analog front-end evaluation kit	*Analog Devices* FMCOMMS1-EBZ
switch	*Analog Devices* HMC8038
power amplifier	*Analog Devices* HMC327
low-noise amplifier	*Mini-Circuits* PMA3-83LN+

References

1. Gupta, A.; Jha, R.K. A Survey of 5G Network: Architecture and Emerging Technologies. *IEEE Access* **2015**, *3*, 1206–1232. [CrossRef]
2. Akyildiz, I.F.; Kak, A.; Nie, S. 6G and Beyond: The Future of Wireless Communications Systems. *IEEE Access* **2020**, *8*, 133995–134030. [CrossRef]
3. Larsson, E.G.; Edfors, O.; Tufvesson, F.; Marzetta, T.L. Massive MIMO for next generation wireless systems. *IEEE Commun. Mag.* **2014**, *52*, 186–195. [CrossRef]
4. Ahmadi, S. *5G NR*, 1st ed.; Chapter 4: New Radio Access Physical Layer Aspects (Part 2); Elsevier: Amsterdam, The Netherlands, 2019; pp. 411–654.
5. Rajatheva, N.; Atzeni, I.; Bjornson, E.; Bourdoux, A.; Buzzi, S.; Dore, J.B.; Erkucuk, S.; Fuentes, M.; Guan, K.; Hu, Y.; et al. White Paper on Broadband Connectivity in 6G. 2020. Available online: https://arxiv.org/pdf/2004.14247.pdf (accessed on 28 November 2021).
6. The 5G Infrastructure Public Private Partnership (5G PPP). European Vision for the 6G Network Ecosystem. 2021. Available online: https://5g-ppp.eu/wp-content/uploads/2021/06/WhitePaper-6G-Europe.pdf (accessed on 28 November 2021).
7. Chen, C.; Guevara, A.P.; Pollin, S. Scaling up distributed massive MIMO: Why and How. In Proceedings of the 2017 51st Asilomar Conference on Signals, Systems, and Computers, Pacific Grove, CA, USA, 29 October–1 November 2017.
8. Zhang, J.; Chen, S.; Lin, Y.; Zheng, J.; Ai, B.; Hanzo, L. Cell-Free Massive MIMO: A New Next-Generation Paradigm. *IEEE Access* **2019**, *7*, 99878–99888. [CrossRef]
9. Ranaweera, C.; Wong, E.; Nirmalathas, A.; Jayasundara, C.; Lim, C. 5G C-RAN with Optical Fronthaul: An Analysis from a Deployment Perspective. *J. Lightw. Technol.* **2018**, *36*, 2059–2068. [CrossRef]
10. Breyne, L.; Torfs, G.; Yin, X.; Demeester, P.; Bauwelinck, J. Comparison Between Analog Radio-over-Fiber and Sigma Delta Modulated Radio-over-Fiber. *IEEE Photon. Technol. Lett.* **2017**, *29*, 1808–1811. [CrossRef]
11. Wang, J.; Jia, Z.; Campos, L.A.; Knittle, C.; Jia, S. Delta-Sigma Modulation for Next Generation Fronthaul Interface. *J. Lightw. Technol.* **2019**, *37*, 2838–2850. [CrossRef]
12. Wu, C.-Y.; Li, H.; Caytan, O.A.E.; Van Kerrebrouck, J.; Breyne, L.; Bauwelinck, J.; Demeester, P.; Torfs, G. Distributed Multi-User MIMO Transmission Using Real-Time Sigma-Delta-over-Fiber for Next Generation Fronthaul Interface. *J. Lightw. Technol.* **2020**, *38*, 705–713. [CrossRef]
13. Wu, C.-Y.; Li, H.; Van Kerrebrouck, J.; Vandierendonck, A.; De Paula, I.L.; Breyne, L.; Caytan, O.; Lemey, S.; Rogier, H.; Bauwelinck, J.; et al. Distributed Antenna System Using Sigma-Delta Intermediate-Frequency-over-Fiber for Frequency Bands Above 24 GHz. *J. Lightw. Technol.* **2020**, *38*, 2765–2773. [CrossRef]
14. Sezgin, I.C.; Aabel, L.; Jacobsson, S.; Durisi, G.; He, Z.S.; Fager, C. All-Digital, Radio-Over-Fiber, Communication Link Architecture for Time-Division Duplex Distributed Antenna Systems. *J. Lightw. Technol.* **2021**, *39*, 2769–2779. [CrossRef]
15. Wu, C.-Y.; Meysmans, C.; Li, H.; Van Kerrebrouck, J.; Caytan, O.; Lemey, S.; Bauwelinck, J.; Demeester, P.; Torfs, G. Demonstration of a scalable distributed antenna system using real-time bit-interleaved sigma-delta-over-fiber architectures. In Proceedings of the 2020 European Conference on Optical Communications (ECOC), Brussels, Belgium, 6–10 December 2020.
16. Ebrahimi, M.M.; Helaoui, M.; Ghannouchi, F.M. Delta-Sigma-Based Transmitters: Advantages and Disadvantages. *IEEE Microw. Mag.* **2013**, *14*, 68–78. [CrossRef]
17. Frappé, A.; Flament, A.; Stefanelli, B.; Kaiser, A.; Cathelin, A. An All-Digital RF Signal Generator Using High-Speed ΔΣ Modulators. *IEEE J. Solid-State Circuits* **2009**, *44*, 2722–2732. [CrossRef]
18. Caytan, O.A.E.; Bogaert, L.; Li, H.; Van Kerrebrouck, J.; Lemey, S.; Torfs, G.; Bauwelinck, J.; Demeester, P.; Agneessens, S.; Ginste, D.V.; et al. Passive Opto-Antenna as Downlink Remote Antenna Unit for Radio Frequency Over Fiber. *J. Lightw. Technol.* **2018**, *36*, 4445–4459. [CrossRef]
19. Li, H.; Breyne, L.; Van Kerrebrouck, J.; Verplaetse, M.; Wu, C.-Y.; Demeester, P.; Torfs, G. A 21-GS/s Single-Bit Second-Order Delta-Sigma Modulator for FPGAs. *IEEE Trans. Circuits Syst. II Express Briefs* **2019**, *66*, 482–486. [CrossRef]
20. IEEE Computer Society LAN/MAN Standards Committee. IEEE Standard for information technology—Telecommunications and information exchange between systems Local and metropolitan area networks—Specific requirements—Part 11: Wireless LAN Medium Access Control (MAC) and Physical Layer (PHY) Specifications—Amendment 4: Enhancements for Very High Throughput for Operation in Bands below 6 GHz. *IEEE Std 802.11.* 2013; pp. 1–425. Available online: https://ieeexplore.ieee.org/servlet/opac?punumber=6687185 (accessed on 28 November 2021).
21. 3GPP TS 38.104. New Radio (NR): Base Station (BS) Radio Transmission and Reception (Release 17) (V17.3.0); September 2021. Available online: https://www.tech-invite.com/3m38/tinv-3gpp-38-104.html (accessed on 28 November 2021).

22. Mody, A.N.; Stüber, G.L. Synchronization for MIMO OFDM Systems. In Proceedings of the GLOBECOM, San Antonio, TX, USA, 25–29 November 2001.
23. Sezgin, I.C.; Gustavsson, J.; Lengyel, T.; Eriksson, T.; He, Z.S.; Fager, C. Effect of VCSEL Characteristics on Ultra-High Speed Sigma-Delta-Over-Fiber Communication Links *J. Lightw. Technol.* **2019**, *37*, 2109–2119. [CrossRef]
24. Common Public Radio Interface (CPRI) Specification V7.0. 2015. Available online: http://www.cpri.info/spec.html (accessed on 28 November 2021).
25. Van De Beek, J.J.; Edfors, O.; Sandell, M.; Wilson, S.K.; Borjesson, P.O. On Channel Estimation in OFDM Systems. In Proceedings of the 1995 IEEE 45th Vehicular Technology Conference. Countdown to the Wireless Twenty-First Century, Chicago, IL, USA, 25–28 July 1995 .